nature physics

LETTERS

PUBLISHED ONLINE: 14 NOVEMBER 2016 | DOI: 10.1038/NPHYS3940

Cooperatively enhanced dipole forces from artificial atoms in trapped nanodiamonds

Mathieu L. Juan[1,2*†], Carlo Bradac[1,2†], Benjamin Besga[1,2], Mattias Johnsson[1,2], Gavin Brennen[1,2], Gabriel Molina-Terriza[1,2] and Thomas Volz[1,2*]

Optical trapping is a powerful tool to manipulate small particles, from micrometre-size beads in liquid environments[1] to single atoms in vacuum[2]. The trapping mechanism relies on the interaction between a dipole and the electric field of laser light. In atom trapping, the dominant contribution to the associated force typically comes from the allowed optical transition closest to the laser wavelength, whereas for mesoscopic particles it is given by the polarizability of the bulk material. Here, we show that for nanoscale diamond crystals containing a large number of artificial atoms, nitrogen–vacancy colour centres, the contributions from both the nanodiamond and the colour centres to the optical trapping strength can be simultaneously observed in a noisy liquid environment. For wavelengths around the zero-phonon line transition of the colour centres, we observe a 10% increase of overall trapping strength. The magnitude of this effect suggests that due to the large density of centres, cooperative effects between the artificial atoms contribute to the observed modification of the trapping strength. Our approach may enable the study of cooperativity in nanoscale solid-state systems and the use of atomic physics techniques in the field of nano-manipulation.

Light forces are key to many cold-atom experiments. Atoms exhibit sharp electronic transitions; these are associated with a pole in the complex atomic polarizability that ultimately enables detuning- and state-dependent optical manipulation. The strength of the optical forces, both reactive and dissipative, can be controlled via detuning of the laser from the atomic resonance. In the case of the reactive dipole force, which is at the centre of this work, the sign of the detuning even determines whether the optical potential associated with the force is repulsive (photon energy larger than the transition energy) or attractive (photon energy smaller than the transition energy). Complex optical near-field traps for cold atoms have been demonstrated[3] as a result of this extra degree of freedom. Introducing detuning-dependent optical manipulation techniques into the field of nano-manipulation by embedding artificial atoms into the nano-objects would therefore open up a whole new range of possibilities. While detuning-dependent forces have been studied for micro-/nanoparticles exhibiting plasmonic resonances or Mie resonances, they are typically several tens of nanometres wide[4]. To engineer sharp Mie resonances[5], large particles are required along with either near-field coupling or complex propagating beams[6] to efficiently excite them. In turn, embedding artificial atoms in the nanoparticle provides spectrally sharp resonances, even at room temperature. In the context of quantum optomechanics with levitated nano-objects[7,8], these forces could enable novel cooling techniques such as Doppler cooling for accessing new parameter regimes. A challenge in applying atomic physics techniques to nanoparticles arises due to the coupling to the environment, which typically leads to dephasing of the artificial atoms within the nanoparticle, greatly reducing the reactive part of the optical force. In our experiment, we find that this detrimental effect of dephasing is indeed present. Remarkably this is overcome to a great extent by cooperative effects. While the impact of cooperativity on different aspects of quantum optics has been extensively studied[9], its impact on optical forces has been theoretically predicted[10,11] but experimental evidence remains limited to light scattering[12] and dissipative forces[13]. We show in our experiment that, due to cooperative effects, the dipole force is enhanced by more than one order of magnitude compared with the force that would be obtained considering independent artificial atoms.

Nanodiamonds containing colour centres are excellent candidate nanoparticles for observing atom-like trapping resonances. In particular, the nitrogen–vacancy (NV) centre, consisting of a nitrogen atom and an adjacent vacancy site (see Fig. 1a left), has attracted a lot of interest over the past decade. In its most stable form, the negatively charged NV^-, it exhibits outstanding spin-optical properties that persist even at room temperature[14]. Consequently, the NV^- has proved to be highly suitable as a solid-state spin qubit and nanoscale magnetic sensor. Here we are mainly interested in its optical properties. The NV^- displays stable single-photon emission with a sharp zero-phonon line (ZPL) in bulk around 637 nm followed by well-defined vibronic side bands. In nanodiamonds, the ZPL position can shift considerably due to lattice strain, and we find a ZPL centred around 639 nm in our experiment. Due to their strong and stable fluorescence, NV^- centres hosted in nanodiamonds have been used as bio-labels for high-resolution, real-time and low-disruption imaging of living cells[15]. Previous investigations on liquid trapping[16,17] and levitating nanodiamonds[18] used laser light at 1,064 nm, which is far away from the ZPL. None of these experiments reported any effects due to the presence of the NV^- centres on the external degrees of freedom of the nanodiamond in the optical trap.

In our experiment, we create a Gaussian standing-wave (GSW) trap[19] near 639 nm by focusing a Gaussian laser beam on a silver-coated mirror. The GSW provides a stronger trap along the direction of the standing wave compared with a conventional focused Gaussian beam. In addition the scattering force, proportional to the difference between the Poynting vectors of the incoming and the reflected beams, can be neglected due to the high reflectivity of the silver mirror. The mirror forms the top of a static microfluidic

[1]Department of Physics & Astronomy, Macquarie University, New South Wales 2109, Australia. [2]ARC Centre of Excellence for Engineered Quantum Systems, Macquarie University, New South Wales 2109, Australia. †These authors contributed equally to this work. *e-mail: mathieu.juan@mq.edu.au; thomas.volz@mq.edu.au

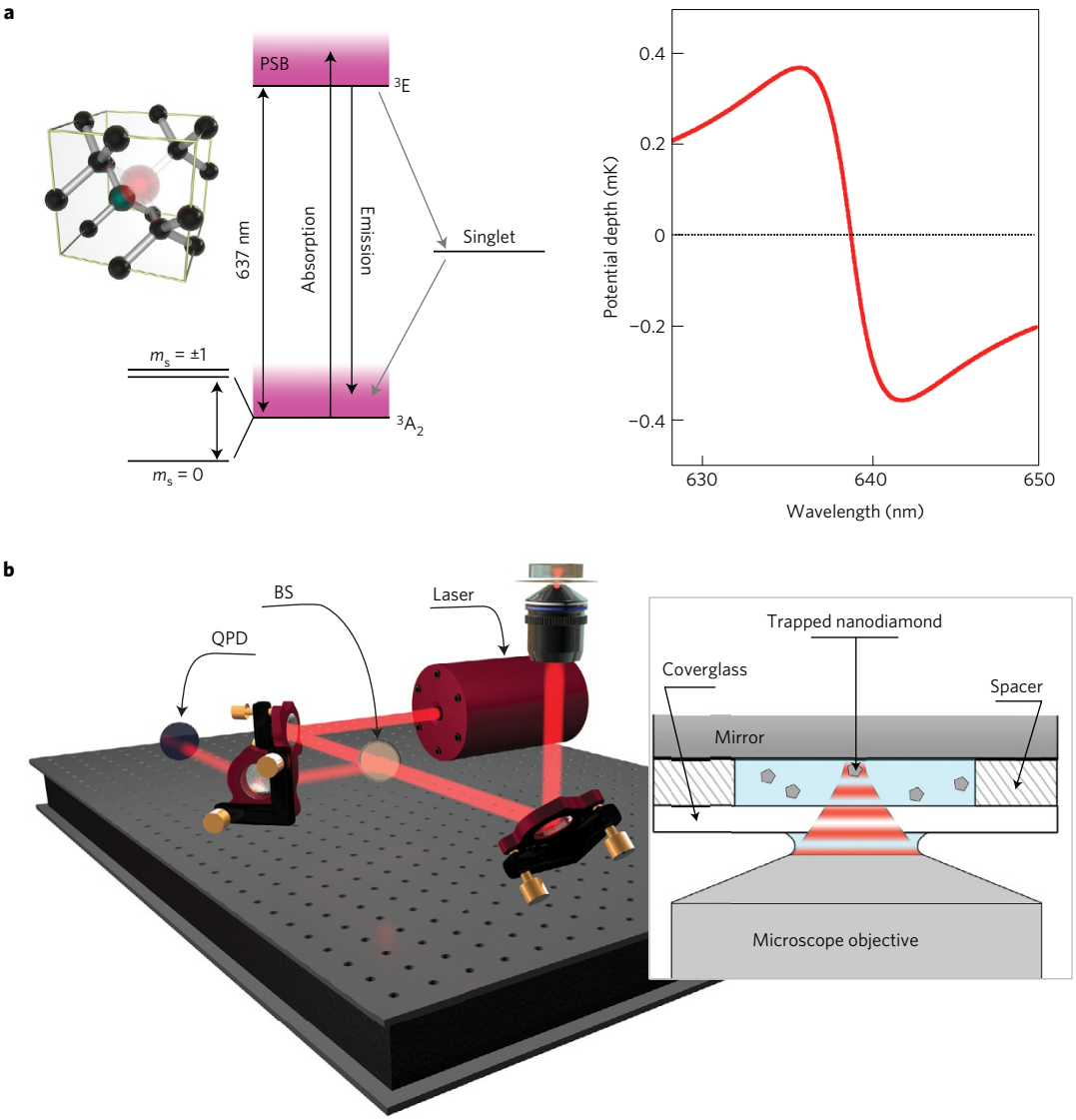

Figure 1 | Trapping nanodiamonds. a, Highly irradiated nanodiamonds contain many nitrogen–vacancy centres that exhibit a strong optical transition at around 637 nm (left panel). The level scheme displays the relevant optical and non-radiative transitions (for spectroscopic notation, see, for example, ref. 14). A single NV centre trapped in the centre of a focused Gaussian beam (numerical aperture 1.2, $P = 4$ mW) experiences a dispersive atom-like trapping potential due to the near-resonant dipole force (right panel). **b**, Experimental set-up with the trapping laser focused through a high-numerical-aperture objective into a microfluidic chamber producing a strong optical trap. The microfluidic chamber (right panel) consists of a coverglass (145-μm thick), a spacer (140-μm thick) and a mirror on the top that results in a standing wave, improving the trapping efficiency and minimizing the scattering force. The light backscattered from the system is collected via a beam splitter (BS) and sent to a quadrant photo-detector (QPD) to track the position of the particle.

chamber that contains the nanodiamonds suspended in deionized water (see Fig. 1b). The laser sources are a set of temperature-stabilized laser diodes operating at different wavelengths detuned with respect to 639 nm (see Methods). In addition, a pulsed green laser (532 nm) serves as a weak re-pump to counteract resonant ionization to the neutral NV^0 state[20]. The nanodiamonds are in the strongly overdamped regime and their displacement from the trap centre is small compared with the beam waist. As a result, the particles mainly probe the harmonic part of the potential near the trap minimum $U \sim U(0) + \kappa x^2$ (ref. 21), where κ is the so-called trap stiffness. Experimentally, the trap stiffness is obtained by recording the (time-dependent) position of the trapped particle on a quadrant photodiode and by extracting the corresponding corner frequency[1] (see Methods and Supplementary Information). Due to its dependence on the size of the trapped nanodiamond, κ cannot be directly compared for different nanodiamonds. To circumvent this problem, we extract a relative value for κ normalized to the measured trap stiffness at a reference wavelength ($\lambda_{ref} = 639.13$ nm) for each nanodiamond separately (see Supplementary Information).

To obtain a significant resonant trapping effect, we use nanodiamonds with a high concentration of NV^- centres[22]. We first characterized the nanodiamonds using a home-built combined confocal/atomic force microscope (AFM) set-up (see Methods). The investigated NV^- centres show a ZPL centred at (639.1 ± 0.7) nm with an average spectral width of (2.1 ± 0.6) nm (see Supplementary Information). The ZPL width of individual nanodiamonds is a convolution of a Gaussian due to the variation of NV ZPL frequency within a nanodiamond and a Lorentzian distribution (Voigt profile). Assuming a dephasing rate at room temperature of approximately $2\pi \times 1$ THz (ref. 23), we extracted the width of the underlying Gaussian distribution to be $\sigma_{ZPL} = (1.8 \pm 0.6)$ nm. At room temperature, most photons are emitted into the phonon sidebands and only a fraction into the ZPL. Using a value of 5% for this branching ratio[24], the dipole moment of the ZPL

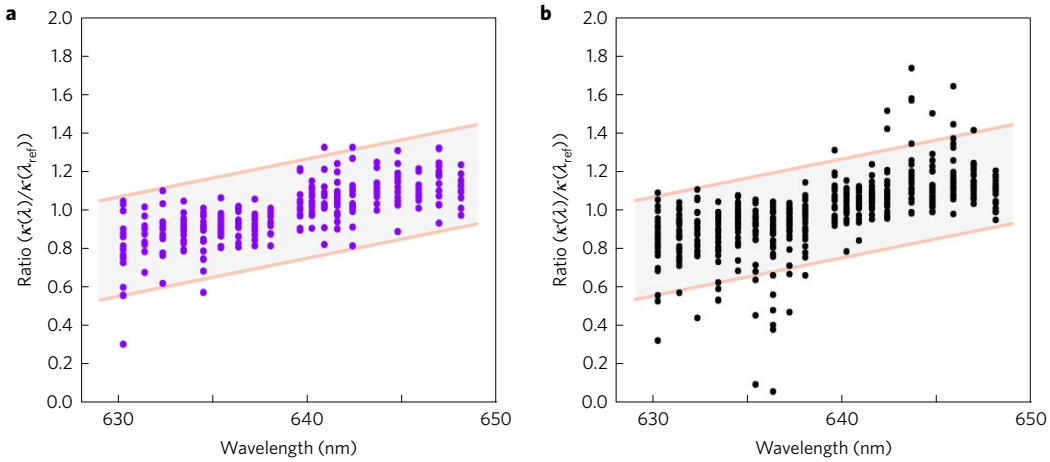

Figure 2 | Measured relative trap stiffness. a, Relative trap stiffness ($\kappa(\lambda)/\kappa(\lambda_{ref})$) for nanodiamonds containing only a few NVs. The symmetric spread in the measured trap stiffness for a given wavelength is due to experimental noise. **b**, Relative trap stiffness for nanodiamonds containing a large number of NV centres. The data scattering is strongly asymmetric with κ-ratios much lower than 1 for wavelengths below λ_{ref} and higher than 1 for wavelengths above λ_{ref}. In **a**,**b**, the shaded areas are guides to the eye obtained using three times the average standard deviation from the low-density NV sample (**b**) with an overall linear trend.

transition amounts to 1.16 D (assuming a total decay time in bulk diamond of 12.5 ns (ref. 23)). We also measured the size distribution of the nanocrystals using the AFM, confirmed using dynamic light scattering of the nanodiamonds in suspension, and found an average size of (150 ± 23) nm. The expected average number of NVs per nanodiamond, $\langle NV \rangle \approx 9{,}500$, was obtained from photoluminescence measurements (see Methods). In our force measurements, we used a reference sample of nanodiamonds with a similar size, (168 ± 31) nm, but with only a few NV centres (on average three NVs per nanodiamond, see Methods).

To characterize the contribution of the NVs to the trap stiffness, we measured the corner frequency on a number of different nanodiamonds for a given set of wavelengths for the two nanodiamond samples (low and high NV centre concentration). We then extracted the trap stiffness for each nanodiamond separately and applied a statistical analysis to systematically discard unwanted events such as the trapping of multiple nanodiamonds or standing-wave hopping (see Supplementary Information). The resulting trap stiffness ratios as a function of laser wavelength for the reference nanodiamonds are displayed in Fig. 2a. This measurement serves as a reference as we do not expect the resonant trapping forces to have a measurable effect for this sample. The monotonic trend is attributed to chromatic aberrations that are aggravated by the standing-wave trap (see Supplementary Information). In contrast, Fig. 2b displays the results for the nanodiamond sample with high NV^- density. As in the case of the reference sample, the underlying monotonic trend is also visible. However, the high-density data show a strongly asymmetrical distribution with κ-ratio values much lower than 1 for wavelengths below λ_{ref} and values larger than 1 for wavelengths larger than λ_{ref}. The extreme values are attributed to nanodiamonds with a larger number of NV centres leading to a significant contribution of the NVs to the trap stiffness.

Next, we extract the mean value from both data sets and plot the difference of the mean values as a function of wavelength (Fig. 3a). Due to the choice of reference wavelength, this difference of mean values gives access to the ratio of the stiffness arising from the NV ensemble to the stiffness from the bare nanodiamond matrix (see Supplementary Information). The dispersive trend expected for atom trapping is visible with stiffness ratio lower than 1 at wavelengths below the ZPL and larger than 1 for wavelengths above, with a magnitude of up to 10%. Most remarkably, these experimental results cannot be accounted for only by assuming independent NVs: the dashed line in Fig. 3a, displaying the expected trap stiffness assuming independent NV centres, was magnified 40 times to be comparable in magnitude with the experimental values. For this model, we used the average values for the ZPL width ($\sigma_{ZPL} = 1.8$ nm), ZPL position (639.1 nm) and the expected number of NV centres per nanodiamond (9,500). When not constraining the number of NV centres, we obtained the best possible fit for 410,000 NVs instead of the estimated 9,500 (see Supplementary Information). Besides this significant difference in magnitude, this independent NV model gives a slowly varying change of the stiffness that does not match our observations. To fully capture the experimental results, we included cooperative effects[25] between the NV centres within a single nanocrystal.

Cooperative effects between NV centres are expected to have a significant impact on the dipole force by modifying both the spontaneous decay rate and the steady-state population. An increase of the decay rate, or superradiance, was independently confirmed in our high-NV-density nanodiamonds through a set of scattering experiments[26]. Due to the large variation in ZPL position in a single nanodiamond, only sub-domains of NVs within narrow frequency windows are expected to act cooperatively. To theoretically describe the cooperatively enhanced forces, we apply the Dicke model[27] to each sub-domain i containing a number N_i of NV centres. The force can then be obtained by solving the Liouville equation for the collective spin operator with a single-spin dephasing rate that is given by the spontaneous decay rate of the NV, and a collective spin dephasing rate at room temperature of $2\pi \times 1$ THz (ref. 23) (see Supplementary Information). The cooperatively enhanced force calculated for our particular nanodiamond sample is presented in Fig. 3a as the solid black line along with the experimental data points. To properly account for the variability in the nanodiamond properties (ZPL position of each NV and number of NVs) we used a Monte Carlo approach with a noise model matching the experimental noise and numerically reproduced our measurements (see Supplementary Information). This provides the expected average effect of the NV centres on the stiffness, but also the 1σ interval where 68.2% of the experimental data points would statistically fall (shaded area in Fig. 3a). For this cooperatively enhanced model, we set the average number of NV centres to the estimated value 9,500 and used the spectral width of the cooperative sub-domains as the only adjustable parameter. The measurements were best reproduced using a sub-domain of approximately 100 GHz corresponding to an average domain size of 95 NV centres, or 1% of the total average number of centres (see Supplementary

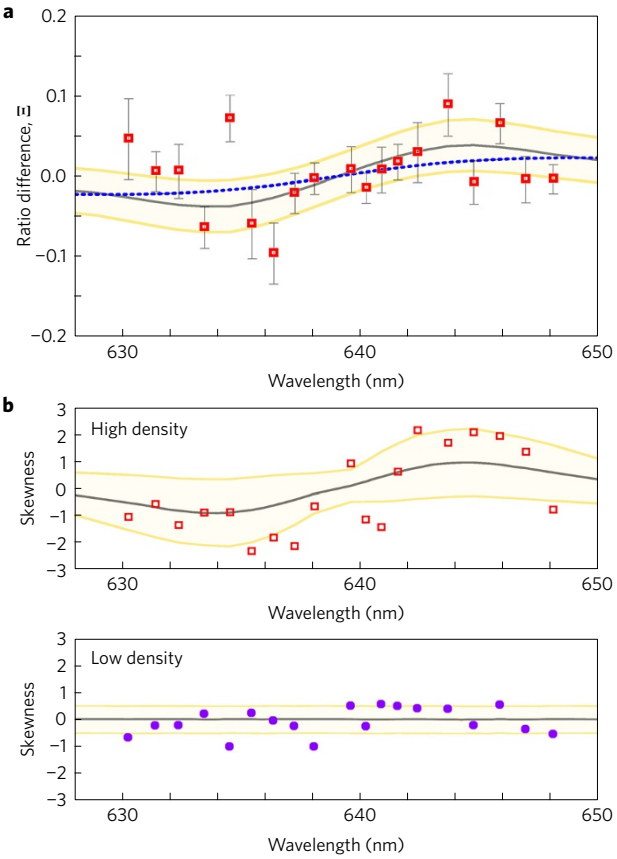

Figure 3 | Cooperative dipole force. a, Difference of the mean values from Fig. 2a and b. This difference, $\Xi = \kappa(\lambda)/\kappa(\lambda_{ref})|_{highNV} - \kappa(\lambda)/\kappa(\lambda_{ref})|_{lowNV}$, is a close approximation of the ratio of the stiffness from the NV centres, $\kappa_{NVs}(\lambda)$, over the stiffness from the diamond matrix, $\kappa_{Diamond}(\lambda)$ (see Methods). The standard error from the experimental data is indicated by the error bars in grey. The black curve shows the theoretically predicted stiffness ratio accounting for cooperative effects on the force obtained for cooperative sub-ensembles with a spectral width of 100 GHz (residual sum of square: 2.4×10^{-2}). For comparison, the dashed line showing the theoretical prediction for independent NVs was magnified 40 times to reach comparable magnitude (residual sum of square: 3.3×10^{-2}). **b**, Skewness as a function of wavelength. Top panel: experimental skewness (open squares) from high-density NV sample measurements. Bottom panel: experimental skewness from the low-density NV sample. In **a**,**b**, the Monte Carlo model was used to obtain an average expected skewness (solid line) as well as the 1σ interval where 68.2% of the experimental value should lie.

Information). It is important to note that we have not explicitly taken into account additional effects that can limit the cooperativity between NV centres. These effects, such as the $NV^0 \leftrightarrow NV^-$ ionization, will directly impact the average size of the cooperative domains and significantly reduce them as they become prevalent. To quantitatively compare the quality of the fits obtained for the two different models, independent and cooperatively enhanced forces, we used the Akaike information criterion[28]. This criterion provides an evidence ratio allowing for the direct comparison of the fit quality from two distinct models. By using the expected average number of NV centres for both models, the evidence ratio for the cooperatively enhanced forces compared with the independent forces is 7.5 while the usual bound for identifying the best model with strong confidence is 2.7 (see Supplementary Information). In terms of magnitude, the cooperatively enhanced model predicts an increase of the stiffness 65 times larger than the model for independent NVs (3.8% compared with 0.06%). In addition, the dispersive shape described by the experimental data is also better fitted by the cooperatively enhanced force model. In parallel to the average trap stiffness, we also modelled the expected skewness along with the 1σ interval (Fig. 3b). Our model is in good quantitative agreement with the skewness obtained from the experiment with the high-NV-density sample. For comparison, the skewness of the experimental data obtained for the reference nanodiamond sample is presented in the lower panel of Fig. 3b.

In conclusion, our observations open the door to a wealth of new research directions. The cooperative effects arising from a large number of NV centres in an individual nanocrystal provide a mechanism to significantly increase the optical forces. While our simplified model is in good agreement with the experiment, a more complete description accounting for dipole–dipole interactions[27] constitutes an interesting future research direction. In addition, the observed change of up to 10% in trap stiffness could be further increased by using defects such as silicon–vacancy centres that are characterized by higher densities[29] and stronger transition dipole moment[30]. These centres could offer the opportunity to access a regime in which the resonant trapping forces would actually dominate the dynamics of the system, with the nanocrystal essentially behaving like a very large atom, or 'superatom'. In the context of quantum optomechanics, this could allow for single-photon strong coupling and sideband cooling at room temperature[31]. In addition, the presence of these quantum emitters could enable state-dependent optical forces that have already been successfully employed, for example, to implement quantum logic gates with atomic ions[32] or create large-scale multiparticle entanglement of neutral atoms in optical lattices[33]. With all of these exciting possibilities at hand, this work opens the door to applying the powerful quantum technologies developed for atom trapping and cooling to the manipulation of small nanoparticles, introducing an unprecedented degree of control at the nanoscale.

Methods

Methods, including statements of data availability and any associated accession codes and references, are available in the online version of this paper.

Received 25 February 2016; accepted 29 September 2016; published online 14 November 2016

References

1. Neuman, K. C. & Block, S. M. Optical trapping. *Rev. Sci. Instrum.* **75,** 2787–2809 (2004).
2. Grimm, R., Weidemüller, M. & Ovchinnikov, Y. B. Optical dipole traps for neutral atoms. *Adv. At. Mol. Opt. Phys.* **42,** 95–170 (2000).
3. Vetsch, E. *et al*. Optical interface created by laser-cooled atoms trapped in the evanescent field surrounding an optical nanofiber. *Phys. Rev. Lett.* **104,** 203603 (2010).
4. Dienerowitz, M., Mazilu, M. & Dholakia, K. Optical manipulation of nanoparticles: a review. *J. Nanophoton.* **2,** 021875 (2008).
5. Li, Y. *et al*. Giant resonant light forces in microspherical photonics. *Light Sci. Appl.* **2,** e64 (2013).
6. Zambrana-Puyalto, X., Vidal, X. & Molina-Terriza, G. Excitation of single multipolar modes with engineered cylindrically symmetric fields. *Opt. Express* **20,** 24536–24544 (2012).
7. Chang, D. E. *et al*. Cavity opto-mechanics using an optically levitated nanosphere. *Proc. Natl Acad. Sci. USA* **107,** 1005–1010 (2010).
8. Romero-Isart, O., Juan, M. L., Quidant, R. & Cirac, J. I. Towards quantum superposition of living organisms. *New J. Phys.* **12,** 033015 (2010).
9. Garraway, B. M. The Dicke model in quantum optics: Dicke model revisited. *Phil. Trans. R. Soc. A* **369,** 1137–1155 (2011).
10. Panat, P. V. & Lawande, S. V. Cooperative effects on optical forces—Dicke's bullet. *Int. J. Mod. Phys. B* **16,** 3787–3795 (2002).
11. Bienaimé, T., Bachelard, R., Piovella, N. & Kaiser, R. Cooperativity in light scattering by cold atoms. *Fortschr. Phys.* **61,** 377–392 (2013).
12. Pellegrino, J. *et al*. Observation of suppression of light scattering induced by dipole–dipole interactions in a cold-atom ensemble. *Phys. Rev. Lett.* **113,** 133602 (2014).

13. Black, A. T., Chan, H. W. & Vuletić, V. Observation of collective friction forces due to spatial self-organization of atoms: from Rayleigh to Bragg scattering. *Phys. Rev. Lett.* **91,** 203001 (2003).
14. Doherty, M. W. *et al*. The nitrogen-vacancy colour centre in diamond. *Phys. Rep.* **528,** 1–45 (2013).
15. McGuinness, L. P. *et al*. Quantum measurement and orientation tracking of fluorescent nanodiamonds inside living cells. *Nat. Nanotech.* **6,** 358–363 (2011).
16. Horowitz, V. R., Alemán, B. J., Christle, D. J., Cleland, A. N. & Awschalom, D. D. Electron spin resonance of nitrogen-vacancy centers in optically trapped nanodiamonds. *Proc. Natl Acad. Sci. USA* **109,** 13493–13497 (2012).
17. Geiselmann, M. *et al*. Three-dimensional optical manipulation of a single electron spin. *Nat. Nanotech.* **8,** 175–179 (2013).
18. Neukirch, L. P., Gieseler, J., Quidant, R., Novotny, L. & Vamivakas, A. N. Observation of nitrogen vacancy photoluminescence from an optically levitated nanodiamond. *Opt. Lett.* **38,** 2976–2979 (2013).
19. Zemánek, P., Jonáš, A., Šrámek, L. & Liška, M. Optical trapping of Rayleigh particles using a Gaussian standing wave. *Opt. Commun.* **151,** 273–285 (1998).
20. Aslam, N., Waldherr, G., Neumann, P., Jelezko, F. & Wrachtrup, J. Photo-induced ionization dynamics of the nitrogen vacancy defect in diamond investigated by single-shot charge state detection. *New J. Phys.* **15,** 013064 (2013).
21. Gieseler, J., Novotny, L. & Quidant, R. Thermal nonlinearities in a nanomechanical oscillator. *Nat. Phys.* **9,** 806–810 (2013).
22. Fu, C. C. *et al*. Characterization and application of single fluorescent nanodiamonds as cellular biomarkers. *Proc. Natl Acad. Sci. USA* **104,** 727–732 (2007).
23. Fu, K.-M. C. *et al*. Observation of the dynamic Jahn–Teller effect in the excited states of nitrogen-vacancy centers in diamond. *Phys. Rev. Lett.* **103,** 256404 (2009).
24. Siyushev, P. *et al*. Low-temperature optical characterization of a near-infrared single-photon emitter in nanodiamonds. *New J. Phys.* **11,** 113029 (2009).
25. Dicke, R. Coherence in spontaneous radiation processes. *Phys. Rev.* **93,** 99–110 (1958).
26. Bradac, C. *et al*. Observation of room-temperature spontaneous superradiance from single diamond nanocrystals. Preprint at https://arXiv.org/abs/1608.03119 (2016).
27. Gross, M. & Harroche, S. Superradiance: an essay on the theory of collective spontaneous emission. *Phys. Rep.* **93,** 301–396 (1982).
28. Burnham, K. & Anderson, D. *Model Selection and Multimodel Inference a Practical Information-Theoretic Approach* (Springer, 2002).
29. Vlasov, I. I. *et al*. Molecular-sized fluorescent nanodiamonds. *Nat. Nanotech.* **9,** 54–58 (2014).
30. Rogers, L. J. *et al*. Electronic structure of the negatively charged silicon-vacancy center in diamond. *Phys. Rev. B* **89,** 235101 (2014).
31. Juan, M. L., Molina-Terriza, G., Volz, T. & Romero-Isart, O. Near-field levitated quantum optomechanics with nanodiamonds. *Phys. Rev. A* **94,** 023841 (2016).
32. Monroe, C., Meekhof, D. M., King, B. E., Itano, W. M. & Wineland, D. J. Demonstration of a fundamental quantum logic gate. *Phys. Rev. Lett.* **75,** 4714–4717 (1995).
33. Mandel, O. *et al*. Controlled collisions for multi-particle entanglement of optically trapped atoms. *Nature* **425,** 937–940 (2003).

Acknowledgements

We thank O. Romero-Isart for useful discussions. This work was funded by the Australian Research Council Centre of Excellence for Engineered Quantum Systems (EQuS) CE 110001013. G.M.-T. acknowledges funding by the Australian Research Council Future Fellowship programme.

Author contributions

M.L.J. and T.V. conceived the research project following the initial idea by T.V. M.L.J., C.B. and B.B. performed the measurements, and M.L.J., C.B., B.B. and T.V. analysed the data. All authors discussed the data. M.L.J., M.J. and G.B. performed the theoretical calculations presented in the manuscript. M.L.J., C.B., G.M.-T. and T.V. wrote the manuscript, and all authors commented on the manuscript.

Additional information

Supplementary information is available in the online version of the paper. Reprints and permissions information is available online at www.nature.com/reprints. Correspondence and requests for materials should be addressed to M.L.J. or T.V.

Competing financial interests

The authors declare no competing financial interests.

Methods

Nanodiamond (ND) sample. The two ND samples used in this work are synthetic type Ib diamond powders with a nitrogen concentration of 300 ppm, that is, 3×10^7 nitrogen atoms per cubic micrometre (Microdiamant MSY 0–0.1 μm). This ND powder was chemically and mechanically processed only to remove the sp^2 carbon phase in excess[34]. These NDs were used with no additional treatment as reference in the control experiment to determine the effect of chromatic aberrations in the standing-wave trap. On average, the untreated NDs contain three NV centres per diamond and in an independent characterization experiment we have not observed diamonds with ten NVs or more. For NDs with a high concentration of NV centres, the ND powder was further treated to increase the concentration of NV centres (Academia Sinica) as follows. The NDs were purified by nitration in concentrated sulfuric and nitric acid (H_2SO_4-HNO_3), rinsed in deionized water, irradiated by a 3-MeV proton beam at a dose of 1×10^6 ions per square centimetre and annealed in vacuum at 700 °C for 2 h to induce the formation of NV centres. Using photoluminescence measurements, 35-nm NDs prepared with this method were estimated to contain 100 NV centres on average[22], or ∼10% of the implanted nitrogen successfully forming an NV defect (∼30 ppm NV density). Using this value, we estimated our sample to contain ∼9.500 NV centres. Prior to the trapping experiment, both ND samples were characterized by means of a laboratory-built confocal scanning fluorescence microscope (100× oil-immersion objective UplanFL N, NA 1.3; Olympus) excited with a 532-nm CW diode-pumped solid-state laser (Compass 315-M100; Coherent Scientific) and combined with a commercial atomic force microscope (Ntegra; NT-MDT)[34]. For characterization, the diamond nanocrystals were dispersed on 145-μm-thick BK7 glass coverslips (BB022022A1; Menzel-Glaser) that were previously sonicated and rinsed in acetone (C3H6O, purity ≥ 99.5%; Sigma-Aldrich) for 10 min. The measured average size of the NDs is (150.5 ± 23.3) nm, determined by atomic force microscopy and confirmed by dynamic light scattering analysis (Zetasizer Nano-ZS; Malvern Instruments). The spectral interrogation of the NDs to identify emission from NV^- centres was performed via a commercial spectrometer (Acton 2500i, Camera Pixis100 model 7515-0001; Princeton Instruments). Using photoluminescence measurements alongside with the size of the NDs obtained from AFM measurements, we extracted the typical variability in the number of NV centres in each ND. This statistical distribution of the NV number was calibrated using the average density of centres provided in ref. 22.

Trapping set-up. For the trapping experiment, the suspension of NDs in deionized water was inserted in a microfluidic chamber consisting of a BK7 glass coverslip (BB022022A1; Menzel-Glaser) and a protected silver mirror (PF10-03-P01; Thorlabs) using double-sided tape for sealing (50 mm × 50 m, 0.14 mm thick; 3M). The experiment involves five diode lasers, four used for the optical trapping itself and one for the re-pumping from NV^0 to NV^-. The re-pump laser is a 532-nm pulsed laser (LDH-P-FA-530B; PicoQuant) used at 40 MHz repetition rate with an average output power at the sample of 30 μW. The four other lasers are temperature-stabilized laser diodes combined through the same fibre to ensure that the focal spots of the different diodes are superimposed perfectly in the lateral direction. One of these diodes is used to provide a stable conventional trap for the ND at a wavelength of 660 nm with 6 mW of power (660 nm/130 mW; Oclaro) to maintain the ND trapped during the measurement. The three remaining diodes provide the reference wavelength (λ_{ref}), the blue and the red wavelengths with 4 mW of power. The choice of diodes (Oclaro 633 nm/110 mW, Oclaro 637 nm/170 mW, Mitsubishi 638 nm/150 mW and Oclaro 642 nm/150 mW) provides an overall covered spectral range of 629–648 nm (see Supplementary Information). The laser beams are switched using home-built electromechanical shutters controlled with a data acquisition system (NI-PCI 6289; National Instruments) to provide 50-s continuous time traces composed of 10-s segments with different wavelengths (see Supplementary Information). The trapping beam at the output of the fibre is polarized using a Glan-Laser calcite polarizer (GL10-A; Thorlabs) and then focused into the chamber through a water-immersion objective (UPLSAPO 60XW, NA 1.2; Olympus) with a measured waist at 640 nm of $w_0 = 470$ nm. The position of the objective is set such that the reference laser diode (639.13 nm) is focused on the mirror forming the top surface of the microfluidic chamber. Finally, the wavelength for the reference laser was chosen very close to the measured average NV ZPL position of 639.08 nm.

Stiffness measurement. Using a quadrant photodiode (PDQ80A, Thorlabs), the position of the ND is tracked over time. A Fourier transform of the signal yields the corresponding power spectral density in reciprocal space. From a Lorentzian fit to the power spectral density[1], the corner frequency f_c is extracted, which can be directly related to the trap stiffness through $\kappa = 2\pi\beta f_c$, where β is the drag coefficient of the ND. In the experiment, we measure f_c as a function of wavelength in the vicinity of the ZPL of the NV^-. The drag coefficient β is a function of the viscosity of the medium, the ND size and its distance to the surface[1]. Consequently, referencing every measurement to a reference wavelength $f_c(\lambda_{measure})/f_c(\lambda_{ref})$ allows direct access to the ratio of the stiffnesses without explicit knowledge of the drag coefficient: $f_c(\lambda_{measure})/f_c(\lambda_{ref}) = \kappa(\lambda_{measure})/\kappa(\lambda_{ref})$. The 50-s continuous time trace provides the corner frequency for: 660-nm only, (λ_{red} + 660-nm), (λ_{blue} + 660-nm), (λ_{ref} + 660-nm) and 660-nm only. Within the harmonic approximation, the overall corner frequency with two lasers on simultaneously (for example, the 660-nm laser and the laser with λ_{ref}) can thus be written as: $f_{ref} = (\kappa_{660} + \kappa_{ref})/(2\pi\beta)$ with β being the drag coefficient of the particular ND. The observables of interest are therefore determined by: $\kappa_{blue}/\kappa_{ref} = (f_{blue} - f_{660})/(f_{ref} - f_{660})$ and $\kappa_{red}/\kappa_{ref} = (f_{red} - f_{660})/(f_{ref} - f_{660})$ (see Supplementary Information for more information).

Stiffness ratio. In the harmonic approximation, the measurement at a given wavelength yields $\kappa_{tot}(\lambda) = \kappa_{NVs}(\lambda) + \kappa_{Diamond}(\lambda)$, where κ_{NVs} is the stiffness related to the NV centres and $\kappa_{Diamond}$ the stiffness related to the diamond matrix. By normalizing with the reference wavelength, we obtain the following ratio:

$$\mathrm{Ratio}(\lambda) = \frac{\kappa_{NVs}(\lambda) + \kappa_{Diamond}(\lambda)}{\kappa_{NVs}(\lambda_{ref}) + \kappa_{Diamond}(\lambda_{ref})} \quad (1)$$

In the case of the low-NV-density NDs, the impact of the NVs on the total force is neglected. As we are interested here in the average values of the stiffness ratio, a difference between these average values can be defined:

$$\Xi(\lambda) = \left\langle \left(\frac{\kappa_{NVs}(\lambda) + \kappa_{Diamond}(\lambda)}{\kappa_{NVs}(\lambda_{ref}) + \kappa_{Diamond}(\lambda_{ref})} \right)_{\text{high NV}} \right\rangle - \left\langle \left(\frac{\kappa_{Diamond}(\lambda)}{\kappa_{Diamond}(\lambda_{ref})} \right)_{\text{low NV}} \right\rangle \quad (2)$$

The choice of the reference wavelength λ_{ref} at the average ZPL was such that the contribution of the NVs to the force is negligible (that is, $\langle \kappa_{NVs}(\lambda_{ref}) + \kappa_{Diamond}(\lambda_{ref}) \rangle \approx \langle \kappa_{Diamond}(\lambda_{ref}) \rangle$). With this approximation, the difference of ratios between high- and low-NV-density NDs simply yields the ratio of the stiffness from the NV centres to the stiffness from the diamond matrix at λ_{ref}:

$$\Xi(\lambda) \approx \left\langle \frac{\kappa_{NVs}(\lambda)}{\kappa_{Diamond}(\lambda_{ref})} \right\rangle \quad (3)$$

Data treatment. As explained previously, the first and last 10 s of the acquisition are necessary to extract the effect of the 660-nm trapping laser only. In addition, we compared the corner frequency for these two segments with the 660-nm trapping laser to identify anomalous events during the whole 50 s of data acquisition. As a boundary condition for discarding anomalous time traces, we imposed a relative change in corner frequency smaller than 10% between the two segments for a trace to be kept. On the basis of this 10% rule, we typically removed 20% of the data. Dramatic changes in 660-nm corner frequency at the beginning and end of the 50-s acquisition period could be related to a second ND hopping into the trap due to the relatively high concentration of NDs in the solution or the hopping of the trapped ND between antinodes of the GSW.

This 10% rule was applied before calculating the trapping stiffness ratios and allowed us to discard clearly anomalous time traces. This rule does not allow one to identify traces for which the corner frequency might have changed during the acquisition but remained the same during the first and last 10 s of acquisition due for example to the intermittent hopping of the ND in the GSW. Such traces will lead to clear outliers in the acquired stiffness ratios. We used a local outlier factor (LOF) method[35] to remove clear statistical outliers from the data. This method is based on calculating the local density of neighbours for each data point. Within the LOF method, (local) outliers are identified by their large LOF value. We rejected data points having a LOF larger than 5.7 using a LOF calculation based on the sixth-nearest neighbour. The same parameters were used for all of the data and ultimately removed 3.4% of the remaining data points (after the 10% rule). We verified that this method would not impact the effect we wanted to detect. To do so, we used the Monte Carlo simulation with the noise model and the cooperative effects to numerically reproduce the experiment accounting only for the variability of the ND properties (number of NVs, average ZPL transition and ZPL standard deviation). Applying the very same LOF selection rule to the numerical results removed only an average 0.8% of the numerical data points. This confirms that even with the large variability in the NV density, the outlier method only marginally impacts the data.

Data availability. The data that support the plots within this paper and other findings of this study are available from the corresponding authors on request.

References

34. Bradac, C., Gaebel, T., Naidoo, N., Rabeau, J. R. & Barnard, A. S. Prediction and measurement of the size-dependent stability of fluorescence in diamond over the entire nanoscale. *Nano Lett.* **9,** 3555–3564 (2009).
35. Breunig, M. M., Kriegel, H.-P., Ng, R. T. & Sander, J. LOF: identifying density-based local outliers. *SIGMOD Rec.* **29,** 93–104 (2000).